INTERNATIONAL JOURNAL OF CLIMATOLOGY
Int. J. Climatol. (2016)
Published online in Wiley Online Library
(wileyonlinelibrary.com) DOI: 10.1002/joc.4623

RMetS
Royal Meteorological Society

Summer Arctic dipole wind pattern affects the winter Siberian High

Bingyi Wu,[a]* Kun Yang[b] and Jennifer A. Francis[c]
[a] *Institute of Climate System, Chinese Academy of Meteorological Sciences, Beijing, China*
[b] *Meteorological Service Office, National Meteorological Center, Beijing, China*
[c] *Department of Marine and Coastal Sciences, Rutgers University, New Brunswick, NJ, USA*

ABSTRACT: This study investigates the relationship between the summer [June–July–August (JJA)] Arctic dipole wind pattern and the following winter [December–January–February (DJF)] Siberian High. It is found that the summer Arctic dipole wind pattern is not confined only to the Arctic region; it spans the large domain north of 20°N. The negative phase of this wind pattern depicts an anomalous anticyclone over the Arctic Ocean and its marginal seas, except for the Barents-Kara seas where an anomalous cyclone is dominant.

This wind pattern is significantly correlated with the strength of the Siberian High during the following winter and with the frequency of extreme cold events over East Asia during the winters of 1979–2014. The relationship of this wind pattern with the winter Siberian High has strengthened over the past decades, particularly since the late 1980s. The more robust relationship coincides with significant changes in the winter atmospheric circulation and frequent occurrences of the negative phase of this wind pattern, which dynamically contributes to low September sea ice extent. The present study's results suggest that autumn Arctic sea ice provides a link between this wind pattern and climate variability over East Asia during the following winter.

Results of simulation experiments suggest that (1) autumn sea ice loss favors the occurrence of a stronger East Asian winter monsoon; (2) the summer Arctic dipole wind pattern modulates winter atmospheric responses to sea ice loss, and the negative phase of this wind pattern enhances the negative feedback of Arctic sea ice loss on winter atmospheric variability over Eurasia and North America. These simulation experiments also imply that complex and varying summer circulation patterns obscure linkages between sea ice loss and large-scale circulation responses over Eurasia. Isolation of the summer Arctic dipole wind pattern, however, provides a potential precursor for the seasonal prediction of winter surface air temperature in a populous region of the world.

KEY WORDS Arctic dipole wind pattern; Siberian High; Arctic sea ice; extreme cold event

Received 30 April 2015; Revised 30 October 2015; Accepted 24 November 2015

1. Introduction

The Arctic sea ice cover has shrunk and thinned since the 1980s (e.g. Stroeve *et al.*, 2012), allowing surface winds to enhance sea ice fracturing and ocean mixing, which promote further melting and expansion of open water (Thorndike and Colony, 1982; Proshutinsky and Johnson, 1997; Rigor *et al.*, 2002; Serreze *et al.*, 2007; Ogi *et al.*, 2010; Spreen *et al.*, 2011; Wu *et al.*, 2012; others). Wind forcing influences spatial distribution of sea ice, sea ice transport out of the Arctic basin into the northern North Atlantic and summer Pacific warm water inflow into the Arctic Ocean, particularly when there is thinner sea ice, which allows stronger wind–ice coupling (Shimada *et al.*, 2006). Previous observations and simulations have also suggested that sea ice thickness variability is controlled partly by wind forcing (Polyakov and Johnson, 2000; Zhang and Hunke, 2001; Holloway and Sou, 2002; Laxon *et al.*, 2003; Ogi *et al.*, 2010; Spreen *et al.*, 2011). Carmack and Melling (2011) indicated that anomalous wind patterns together with the ice-albedo feedback played crucial roles in the rapid loss of Arctic sea ice in recent years.

Anomalously low September sea ice extents are usually associated with the negative phase of the Arctic dipole (AD) wind pattern and the positive phase of the Central Arctic wind pattern during the summer (July–September) season (Wu *et al.*, 2012). The former is associated with a couplet of anomalous high/low pressure centres over the Arctic Ocean/Barents-Kara seas, and the latter corresponds to anomalous high/low pressure centres over the Arctic Ocean/northern Eurasia. It should be noted that the AD wind pattern differs from the widely discussed AD anomaly derived from an empirical orthogonal function (EOF) analysis of sea-level pressure (SLP) variability north of 70°N (Wu *et al.*, 2006), though the AD anomaly is thought to have contributed to record minima of September sea ice extents (Wang *et al.*, 2009). In fact, the AD wind pattern is closely related to EOF3 of SLP variability over the Arctic region (Wu *et al.*, 2012, 2014). Arctic surface wind patterns drive September sea ice extent minima through their frequency and intensity, and increased frequency (positive phase) and strengthened

* Correspondence to: B. Wu, Institute of Climate System, Chinese Academy of Meteorological Sciences, No. 46, Zhong-Guan-Cun South Avenue, 100081, Beijing, China. E-mail: wby@cams.cma.gov.cn

intensity of the Central Arctic wind pattern have contributed substantially to the observed negative trend in September sea ice extent. Certainly, in addition to wind forcing and albedo feedback, summer Arctic sea ice loss is also partly attributed to increased air temperature, changes in ocean currents and sea-water temperature, radiative flux and the preceding winter sea ice loss (Shimada *et al.*, 2006; Polyakov *et al.*, 2010; Lee, 2014; Park *et al.*, 2015). Park *et al.* (2015) showed that strong mid-latitude circulation effects drive enhanced horizontal atmospheric moisture and sensible heat into the Arctic, resulting in increased Arctic downward infrared radiation that, in turn, is responsible for a significant part of the winter sea ice reduction. Arctic sea ice loss and the resulting Arctic amplification affect weather patterns and climate variability over the mid- and high-latitudes (Alexander *et al.*, 2004; Deser *et al.*, 2004; Magnusdottir *et al.*, 2004; Honda *et al.*, 2009; Overland and Wang, 2010; Petoukhov and Semenov, 2010; Screen and Simmonds, 2010; Wu *et al.*, 2011, 2013; Francis and Vavrus, 2012, 2015; Liu *et al.*, 2012; Tang *et al.*, 2013; Cohen *et al.*, 2014; Mori *et al.*, 2014; Kug *et al.*, 2015). On interannual and decadal time scales, associations between Arctic sea ice loss and Eurasian winter climate variability are different (Wu *et al.*, 2011; Yang and Wu, 2013; He *et al.*, 2015).

The Siberian High (SH), as an important action centre of the mid- and high-latitudes of the Northern Hemisphere, has considerable influence on cold waves, the East Asian winter monsoon (EAWM) (Ding, 1990; Wu and Wang, 2002; Jhun and Lee, 2004) and occasional severe cold snaps over parts of Europe. An example is the winter of 2011/2012 when more than 700 people died in Europe because of extreme cold conditions. Several studies suggest that Arctic sea ice loss strengthens the SH in subsequent months, leading to frequent cold winters over East Asia (Honda *et al.*, 2009; Petoukhov and Semenov, 2010; Wu *et al.*, 2011, 2013; Liu *et al.*, 2012; Tang *et al.*, 2013; Cohen *et al.*, 2014; Mori *et al.*, 2014; Kug *et al.*, 2015; Nakamura *et al.*, 2015). However, some recent studies do not find consistently robust linkages between sea ice loss and large-scale circulation anomalies (Screen and Simmonds, 2013a, 2013b; Screen *et al.*, 2014; Overland *et al.*, 2015; Perlwitz *et al.*, 2015; Wu *et al.*, 2015).

This uncertainty highlights the need for the further study of associations between Arctic sea ice variability during summer/fall and high-latitude wind patterns, particularly the possible connection to atmospheric circulation variability over Eurasia during the subsequent winter. Investigating their linkage, therefore, has important implications for the seasonal prediction of winter surface air temperature in a populous region of the world.

2. Data and methods

The following datasets were used in this study: (1) the monthly Arctic sea ice concentration (SIC) from 1979 to 2013 on a $1^\circ \times 1^\circ$ grid, obtained from the British Atmospheric Data Centre (BADC, http://badc.nerc.ac.uk/data/hadisst/); (2) the monthly mean SLP, surface air temperature (SAT), surface winds (10 m) and geopotential heights from January 1979 to February 2014, obtained from the National Centers for Environmental Prediction/National Centers for Atmospheric Research (NCEP/NCAR) Re-analysis I (http://iridl.ldeo.columbia.edu/SOURCES/.NOAA/.NCEP-NCAR/.CDAS-1/.MONTHLY/); and (3) daily SATs from 1 January 1979 to 28 February 2014, obtained from the NCEP/NCAR Re-analysis I.

To extract the dominant patterns of Arctic surface wind variability, complex vector empirical orthogonal function (CVEOF) analysis was applied on the area-weighted normalized monthly mean surface winds north of 50°N from January 1979 to December 2013 (420 months). The CVEOF method itself divides anomalous wind fields into a series of orthogonal wind patterns that are ranked in order of magnitude of the anomalous kinetic energy (see Appendix of Wu *et al.*, 2012). Thus, each wind pattern corresponds to an anomalous kinetic energy of specific spatial variability in the anomalous wind fields. Each wind pattern consists of two sub-patterns that are characterized by the real and imaginary parts of its complex principal component; that is, they determine amplitude (or intensity) and positive/negative polarities of two sub-patterns. Thus, the CVEOF method is superior to EOF from a purely dynamical perspective for characterizing the variety and complexity of climate variability. Detailed information about the method is available in a study conducted by Wu *et al.* (2012).

The Monte Carlo method was applied to examine statistical field significance. For an anomalous field derived from linear regression, the percentage of grid points that are statistically significant at the 0.05 (or 0.01) level is first identified over a domain. This process is then repeated 1000 times with a different series of 35 numbers randomly selected from a normal distribution. The anomalous field is deemed significant if the percentage of significant grid points exceeds that derived from 1000 experimental replications. Additionally, the student's *t*-test was used to assess the statistical significance of atmospheric changes between different phases. Winter daily extreme cold events were defined as winter daily SAT anomalies < -1.5 standard deviation (SD), similar to Thompson and Wallace (2001).

The ECHAM5 (Roeckner *et al.*, 2003) model (T63 spectral resolution and 19 pressure levels) was applied to explore the impact of the initial summer atmospheric conditions on the response of the model atmosphere to the observed sea ice loss forcing in the Northern Hemisphere. The present study used a relatively high horizontal resolution model relative to some previous simulation experiments, such as those with the NCAR Community Atmosphere Model (CAM) version 3 (Alexander *et al.*, 2004; Deser *et al.*, 2004; Magnusdottir *et al.*, 2004; Screen *et al.*, 2014).

3. Summer AD wind pattern and linkages with winter SH: observational analysis

To analyse the potential connections between the summer AD wind pattern and the following winter atmospheric

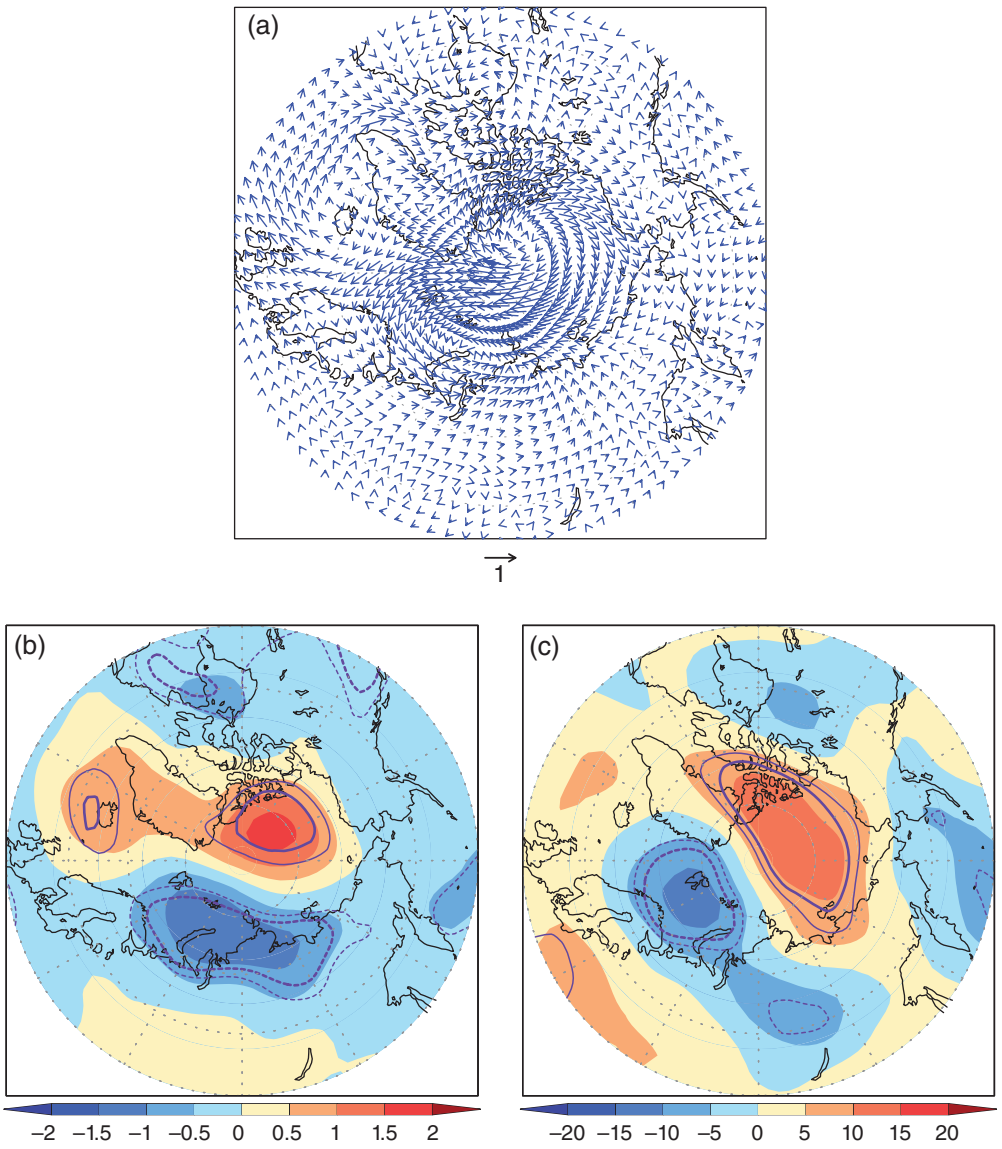

Figure 1. Summer (JJA) mean anomalies in (a) 10-m wind (m s^{-1}), (b) SLP (hPa) and (c) 1000–500 hPa thickness (gpm). Values are derived from linear regression on the normalized negative AD wind pattern using detrended data. In (b) and (c), the thin and thick purple contours indicate anomalies exceeding the 0.05 and 0.01 significance levels, respectively. The AD wind pattern was derived from the leading CVEOF over the domain north of 50°N.

variability over the mid- and high-latitudes of the Asian continent, the CVEOF was applied to extract the predominant wind patterns of monthly mean surface wind variability over the high-latitudes north of 50°N. The leading wind pattern accounts for 16% of the total anomalous kinetic energy for the period 1979–2013 and consists of two sub-patterns known as the AD and northern Laptev Sea (NLS) wind patterns, similar to those in Wu *et al.* (2012). Figure 1 presents regression maps of the summer mean anomalies of surface wind, SLP and 1000–500 hPa thickness. When the AD wind pattern is in its negative phase, an anomalous anticyclone appears over the Arctic Ocean and its marginal seas, except for over the Barents-Kara Seas where cyclonic anomalies dominate (Figure 1(a)). Corresponding summer SLP anomalies show a dipole structure (Figure 1(b)), dynamically consistent with the spatial distribution of surface wind anomalies. The 1000–500 hPa thickness anomalies, which approximately reflect the average air temperature in the low-to-middle troposphere, also exhibit opposing anomalies over the Arctic Ocean and the Nordic Seas (Figure 1(c)).

The summer AD wind pattern is significantly correlated with the ensuing winter [December–January–February (DJF)] SLP and SAT variability over Eurasia (Figure 2). The negative phase of the AD wind pattern corresponds to significant positive SLP anomalies over most of the Asian continent, indicating a strengthened winter SH and EAWM (Figure 2(a)) that results in anomalously cold winter temperatures in East Asia and warm temperatures over much of the Arctic (Figure 2(b)). The winter SH index (SHI) is defined as the regionally averaged SLP over the region bounded by 40°–60°N and 80°–120°E (Wu and Wang, 2002). The AD wind pattern is significantly anticorrelated with the SHI (Figure 2(c): $r = -0.48$ at the 0.05 level,

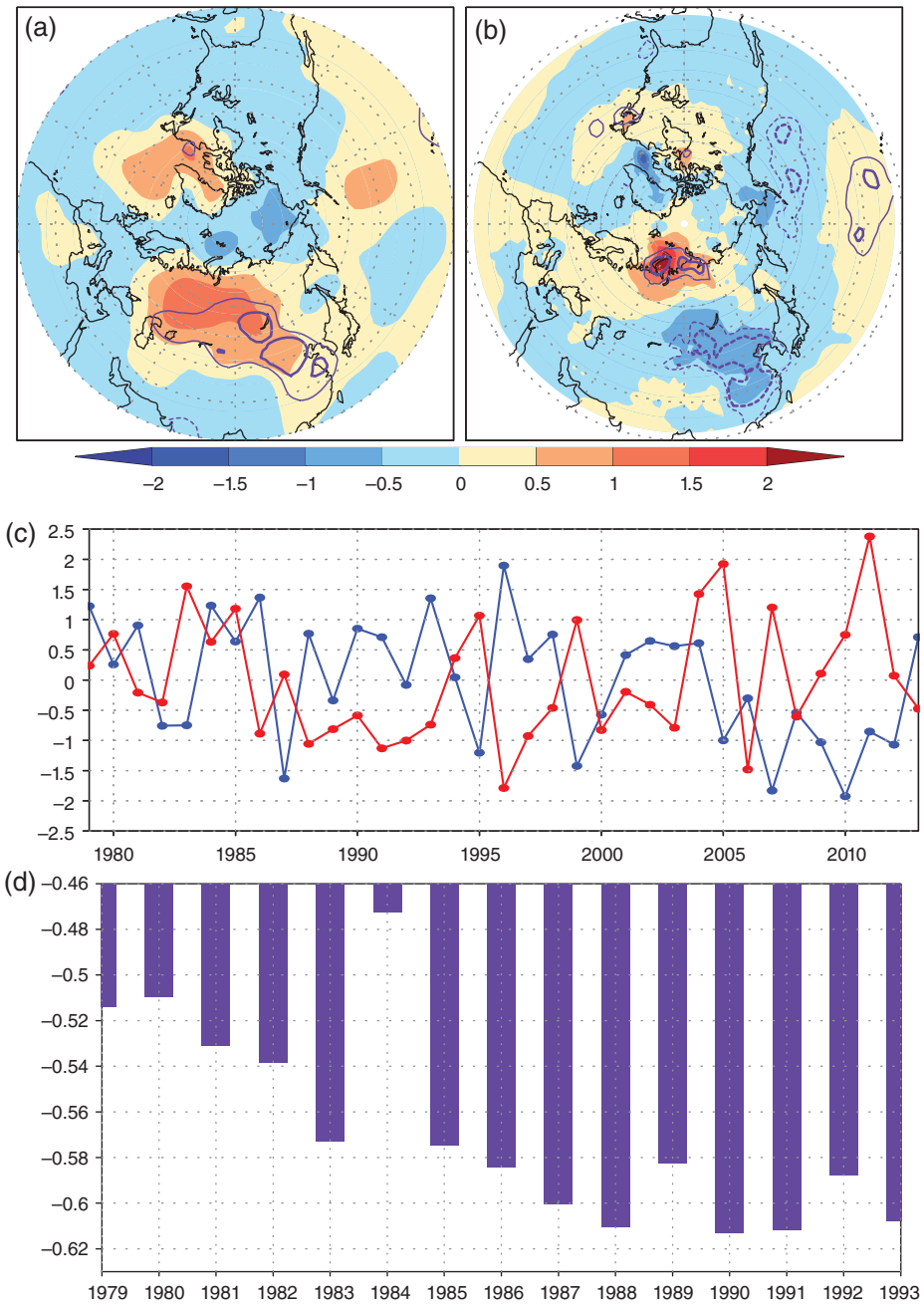

Figure 2. Winter (DJF) mean (a) SLP and (b) SAT anomalies derived from linear regressions on the normalized negative AD wind pattern. Data were detrended before performing linear regression analyses. The thin and thick purple contours indicate anomalies exceeding the 0.05 and 0.01 significance levels, respectively. (c) Normalized time series of the AD wind pattern (blue line) and ensuing winter Siberian High intensity index (SHI, red line): $r = -0.48$. (d) Time series of a 21-year sliding correlation coefficient between the AD wind pattern and ensuing winter SHI. The year on the axis indicates the start year for calculating the 21-year sliding correlation coefficient; for example, '1979' represents the correlation coefficient from 1979 to 1999.

i.e., the one relevant to the observed autocorrelation). The correlation ($r = -0.48$) implies that the AD wind pattern explains less than one quarter of the variance, indicating that over the domain north of 50°N, the AD wind pattern accounts for a modest amount of predictability.

These findings imply that when the phase of the summer AD wind pattern is negative (positive), an anomalous surface anticyclone (cyclone) and positive (negative) thickness anomalies prevail over the Arctic Ocean and its marginal seas in summer. During the winter, following a negative (positive) AD wind pattern, the SH tends to be stronger (weaker). Consequently, the winter SH 'remembers' the preceding summer AD wind pattern and the corresponding thermal anomalies over the Arctic. To further examine this relationship, sequential 21-year sliding correlation coefficients between the AD wind pattern and ensuing winter SHI were calculated (Figure 2(d)). It is apparent that the relationship has strengthened over past decades, particularly since the late 1980s, with negative correlation coefficients remaining stronger than −0.58.

The strengthened relationship coincides with significant changes in the winter atmospheric circulation, that is, the SLP over the Central Arctic has decreased, and the polar vortex throughout the troposphere has weakened substantially since the late 1980s (Walsh *et al.*, 1996) along with opposite trends in winter SAT over the Arctic and the Asian continent (Cohen *et al.*, 2012; Wu *et al.*, 2013). Simmonds (2015) analysed SLP trends in the northern mid- and high-latitudes and showed that strengthening of the summer SLP dipole pattern in the high-latitudes, with anomalous low/high pressure centres over the northern Eurasia/North America, is concurrent with positive trends in the winter SH. Other evidence suggests that the winter tripole wind pattern (a dominant winter weather pattern) over Eurasia has also occurred more frequently since the late 1980s, associated with Arctic sea ice loss (Wu *et al.*, 2013).

Similar analyses were performed over two distinct domains: north of 70°N and north of 20°N. The AD wind patterns are similar and significantly correlated with that derived from the region north of 50°N, with correlation coefficients at 0.87 and 0.98 (after detrending). This implies that the Arctic Oscillation (AO, also known as northern annular mode) cannot be the leading pattern of climate variability from a dynamic perspective, consistent with previous studies (Wu *et al.*, 2012, 2014). If the domain selected is north of 70°N (north of 20°N), the correlation between the summer AD wind pattern and the ensuing SHI is −0.62 (−0.39) after detrending. For the domain north of 70°N, after accounting for the autocorrelation between the two time series, the correlation is −0.62 at the 0.01 significance level.

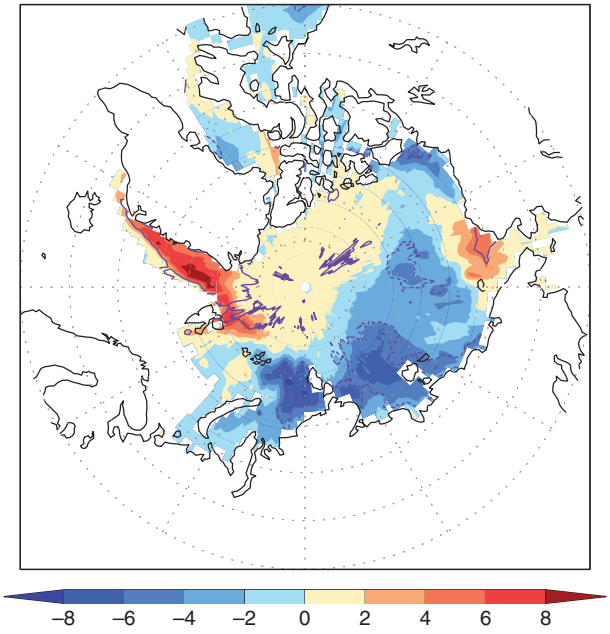

Figure 3. Autumn sea ice concentration (SIC) anomalies (%) derived from linear regression on the normalized negative summer AD wind pattern using detrended data. Contours represent the 0.05 significance level.

4. Possible mechanisms for the linkage

Autumn Arctic SIC may act as the link between the summer AD wind pattern and the following winter SH. Corresponding to the negative phase of the AD wind pattern, significant decreases in autumn SICs are observed from the Kara Sea eastwards to the East Siberian Sea, with opposing SIC anomalies in the Greenland Sea (Figure 3). This spatial distribution is dynamically consistent with an anomalous anticyclone covering the Arctic Ocean and Siberian marginal seas in the preceding summer (i.e., negative AD phase), which enhances the flow of sea ice from the Pacific sector of the Arctic, across the North Pole and out into the Atlantic where it melts (Kwok, 2009; Wu *et al.*, 2012; Zhang *et al.*, 2013). A strongly negative AD wind pattern (SD below −0.5) occurred in the summers of 1982, 1983, 1987, 1995, 1999, 2000, 2005, 2007, 2008, 2009, 2010, 2011 and 2012 (Figure 2(c)). Most of these years occur after the late 1980s, and six out of 13 are since 2007, coinciding with low September sea ice extent during the last decade. The area-weighted, regionally averaged, autumn (SON) SIC in the region bounded by 70.5°–83.5°N and 60.5°–150.5°E was calculated, and it was found that the SIC index is significantly correlated with the AD wind patterns over the three domains after detrending: 0.48 (north of 70°N), 0.46 (north of 50°N) and 0.42 (north of 20°N). These correlations suggest that the negative phase of the AD wind pattern contributes to reduced sea ice during autumn.

Earlier studies proposed mechanisms linking Arctic sea ice loss with changes in the winter atmosphere, including a possible stratosphere–troposphere interaction (Jaiser *et al.*, 2013; Cohen *et al.*, 2014; Kim *et al.*, 2014; Nakamura *et al.*, 2015). Another possibility is a negative feedback mechanism involving Arctic sea ice loss in autumn (Alexander *et al.*, 2004; Deser *et al.*, 2004; Magnusdottir *et al.*, 2004; Wu *et al.*, 2011; and others), which leads to larger heat fluxes from the ocean to the overlying atmosphere, thereby strengthening atmospheric baroclinicity and instability (Deser *et al.*, 2004; Overland and Wang, 2010). Baroclinic processes are then gradually replaced by barotropic processes over high-latitudes, resulting in positive SLP and 500 hPa height anomalies developing over high latitudes that favour a strengthened SH. Additionally, sea ice loss in both autumn and winter contributes to a decrease in the poleward thermal gradient between the Arctic and the mid and high-latitudes of Eurasia, leading to weakened westerlies in winter (Wu *et al.*, 2011; Francis and Vavrus, 2012, 2015) that favour cold air outbreaks southwards from the Arctic.

As a case in point, the present study compares conditions during the summer of 2011, when the AD wind pattern was low (below −0.85) and the SHI reached its maximum, to the situation in 1996, when the wind pattern was the highest value and the SHI was at its minimum (Figure 2(c)). During the summer of 2011, anticyclonic winds dominated the region from the Beaufort Sea clockwise to the Barents Sea (Figure 4(a)), which transferred sea ice from the

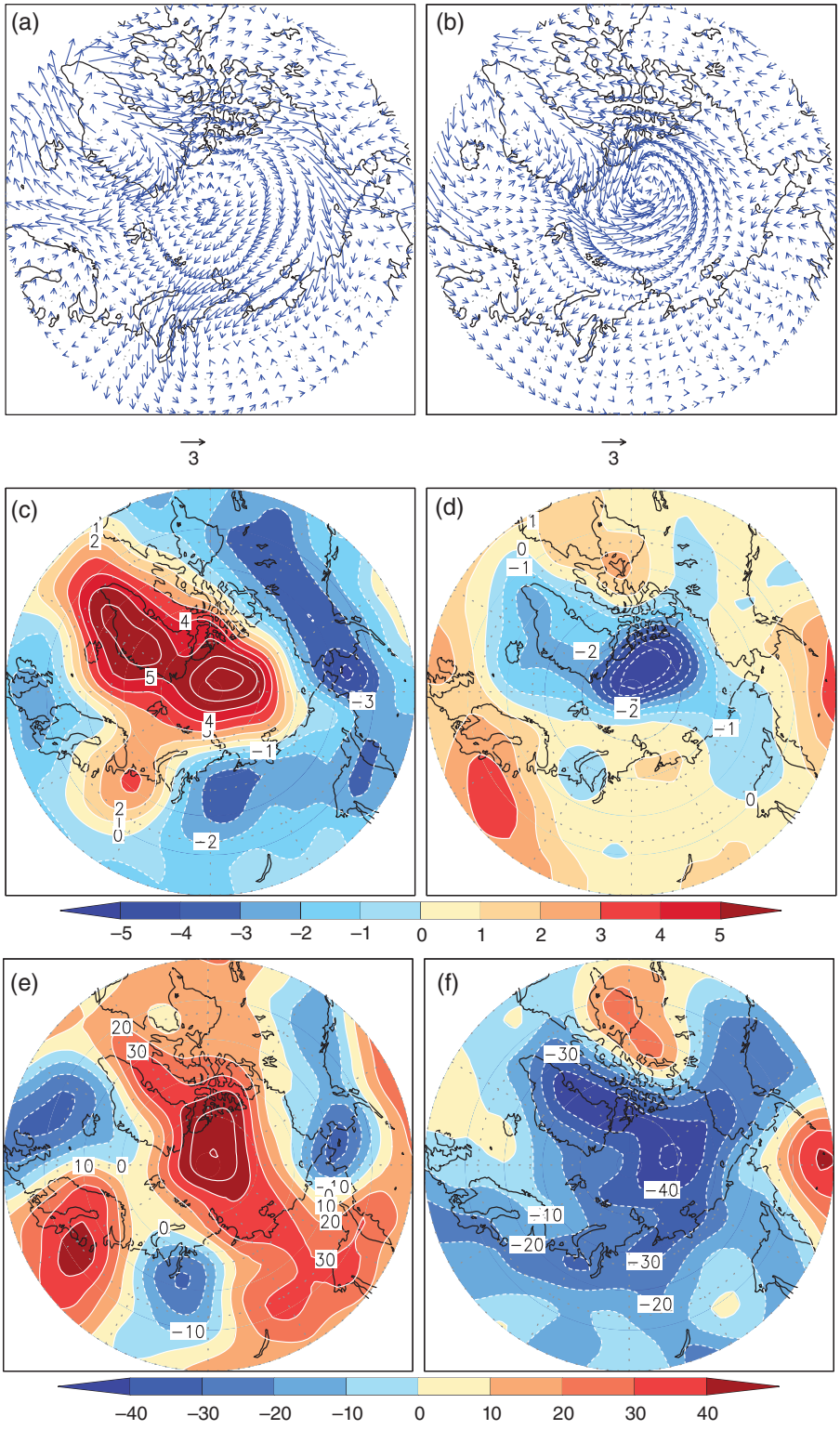

Figure 4. Summer mean 10-m wind fields (m s^{-1}) in (a) 2011 and (b) 1996. (c) and (d): as in (a) and (b), but for summer SLP anomalies (hPa) relative to the mean from 1979 to 2013. (e) and (f): as in (c) and (d), but for summer 1000–500 hPa thickness anomalies (gpm).

western Arctic into the eastern Arctic, that is, moving into warmer water. Meanwhile, positive anomalies in SLP and 1000–500 hPa thickness existed over most of the Arctic Ocean (Figure 4(c) and (e)). In the ensuing autumn, negative SIC anomalies emerged in the Eurasian marginal seas (Figure 5(a)), and the SHI reached a record high value in the winter of 2011/2012 (Figure 2(c)). In the summer of 1996, in contrast, atmospheric circulation anomalies were nearly opposite to those in 2011 (Figure 4(b), (d) and (f)), accompanied by positive SIC anomalies in most of the Siberian marginal seas during autumn (Figure 5(b)). The SH was substantially weaker than normal in the ensuing

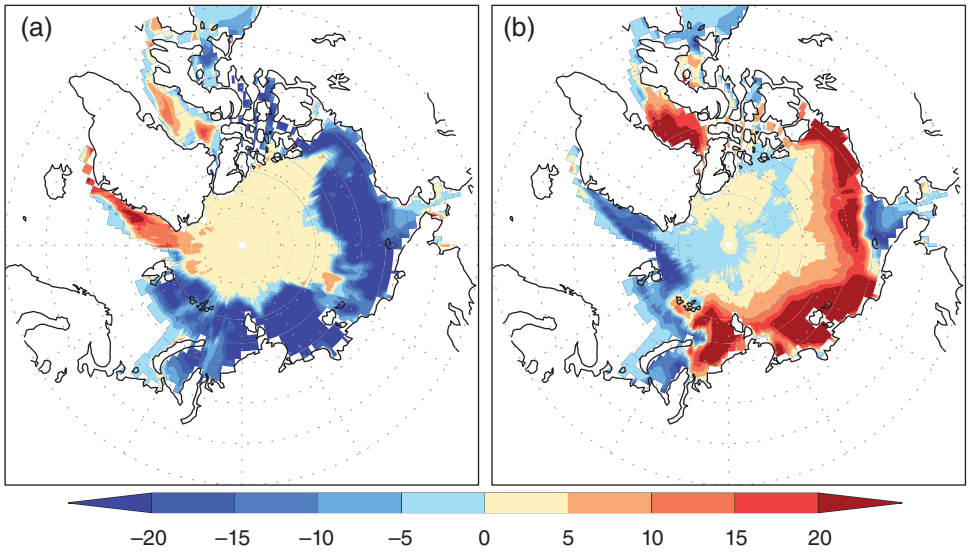

Figure 5. Autumn SIC anomalies in (a) 2011 and (b) 1996 relative to the mean from 1979 to 2013.

winter. Results shown in Figures 1, 2 and 4 imply that when the average air temperature in the low-to-middle troposphere is higher than normal over the Arctic during summer, the winter SH tends to be stronger. The spatial distribution of correlation between the SHI and the preceding summer 1000–500 hPa thickness also support this result (not shown).

5. Model simulations of atmospheric response to sea ice forcing: roles of atmospheric initial conditions

To investigate possible linkage between the summer AD wind pattern and the following winter's atmospheric responses, two sets of simulation experiments were conducted. The first is light sea ice (LICE) experiments with different atmospheric initial conditions that correspond to the summer anomalous cyclone (AC) and anticyclone (AA) over the Arctic Ocean and its marginal seas, which represent the positive and negative phases of the AD wind pattern. For the LICE experiments, SIC data in the Northern Hemisphere were prescribed using observed monthly SIC data from August 2011 to March 2012, while the SIC in the Southern Hemisphere and global sea surface temperature (SST) were prescribed as their climatological monthly mean. The SST and SIC data were obtained through a spatial interpolation of observations; for detailed information, refer to the Atmospheric Model Intercomparison Project (AMIP) II SST and SIC boundary condition data set (http://www-pcmdi.llnl.gov/projects/amip/AMIP2EXPDSN/BCS/bcsintro.php). The heavy sea ice (HICE) experiments were the same as the LICE experiments except that observed monthly SIC data from August 1996 to March 1997 were prescribed as the boundary conditions.

Different atmospheric initial conditions were derived from a spatial interpolation of the NCEP/NCAR daily re-analysis I during summertime (JJA) (92 days each summer) in 1996 (AC initial conditions) and 2011 (AA initial conditions). Variables included surface pressure, air temperature, divergence, vorticity and specific humidity. For both the LICE and HICE cases, 92 simulations were conducted with the AA and AC initial conditions, and the model was run from August to March of the next year. This large number of realizations allowed robust significance testing and statistical analysis. In regions where the SIC changed, the SST was prescribed at its climatological value.

Figure 6 presents differences in ensemble means between the LICE/AA (2011) and the HICE/AC (1996) (former – latter). Positive SLP anomalies are simulated over most of Eurasia and northern North Pacific, the Arctic Ocean and northern North Atlantic along with negative SLP anomalies over all of North America and Asian low-latitudes (Figure 6(a)). Some separated areas where positive SLP differences exceed the 0.05 significance level, including central Eurasia and East Asia, were observed. Negative SAT anomalies occupy most of Eurasia, the northwest North Pacific and parts of the Arctic Ocean/North America, with strong positive SAT anomalies over the Greenland Sea eastward to the Laptev Sea and eastern North America (Figure 6(b)). Compared with SLP differences, SAT differences are more robust. Significant negative SAT anomalies are evident over the mid- and low-latitudes of Eurasia, northeast Asia, the Far East of Russia, the northern North Pacific and a part of the Arctic Ocean. Significant positive SAT anomalies appear over high-latitudes, eastern North America and the northwestern Pacific sector. A comparison with observed SLP and SAT anomalies (Figure 6(c) and (d); note differences in scale) suggests that model simulations capture most major anomaly patterns, although differences are also apparent. For example, positive SLP anomalies in the eastern North Atlantic are absent in simulations, and positive SLP anomalies in the northeastern Pacific and over much of the Arctic are stronger in the simulations.

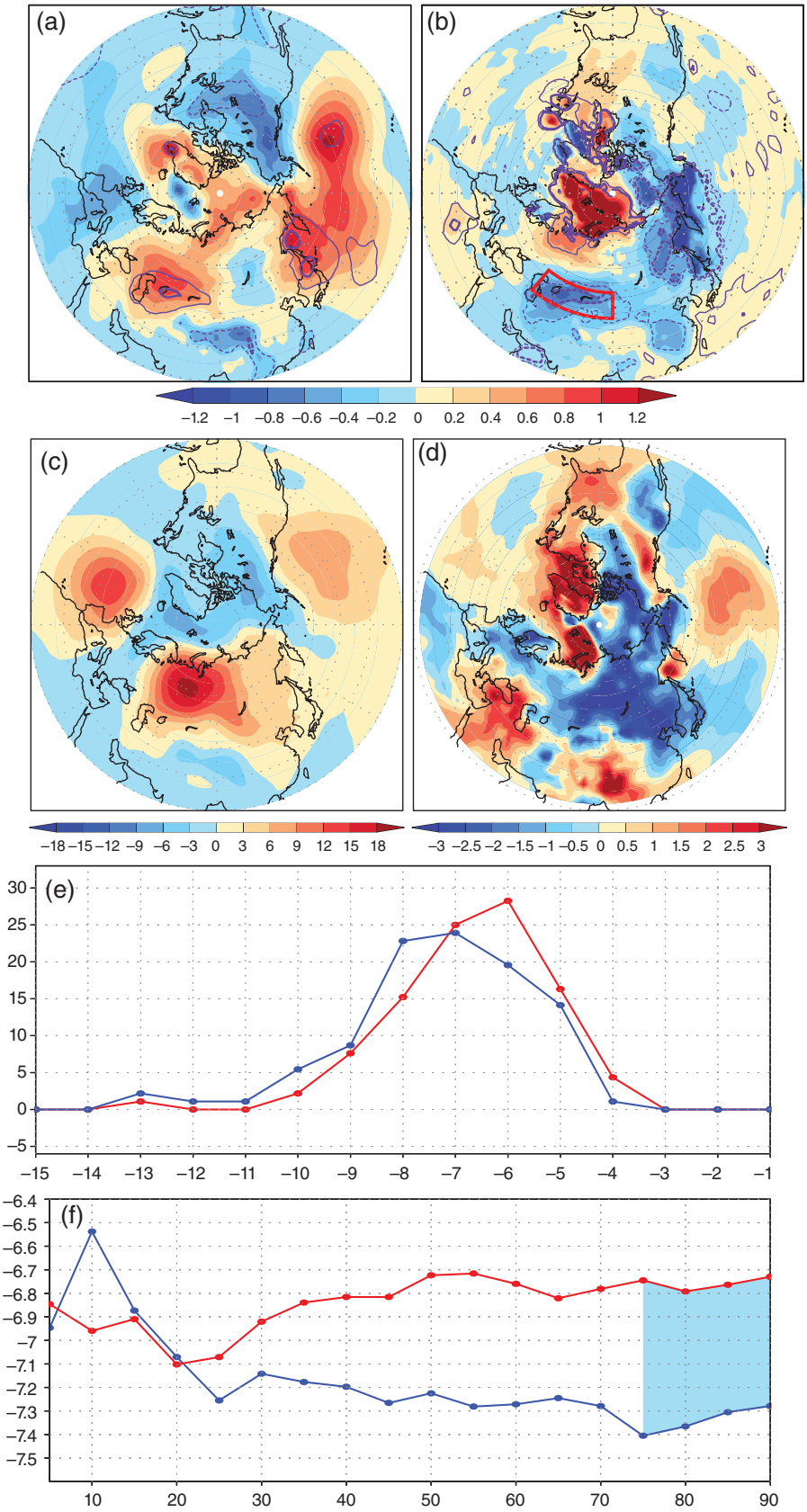

Figure 6. Winter (a) SLP (hPa) and (b) SAT (°C) differences in ensemble means between the LICE/AA and the HICE/AC experiments (former − latter). The thin and thick purple contours represent differences at the 0.05 and 0.01 significance levels, respectively. Observed winter mean (c) SLP and (d) SAT differences between 2011/2012 and 1996/1997 (former − latter). (e) Probability distribution curves (%) of simulated winter mean SATs in the domain in (b) (outlined in red) for the LICE/AA (blue) and the HICE/AC (red) experiments. (f) Evolutions of the regionally (outlined in red) averaged winter SATs with ensemble member numbers; the red and blue curves respectively indicate the HICE/AC and LICE/AA experiments, and the shading area denotes differences in winter mean SATs between the two sets of experiments at the 0.05 significance level.

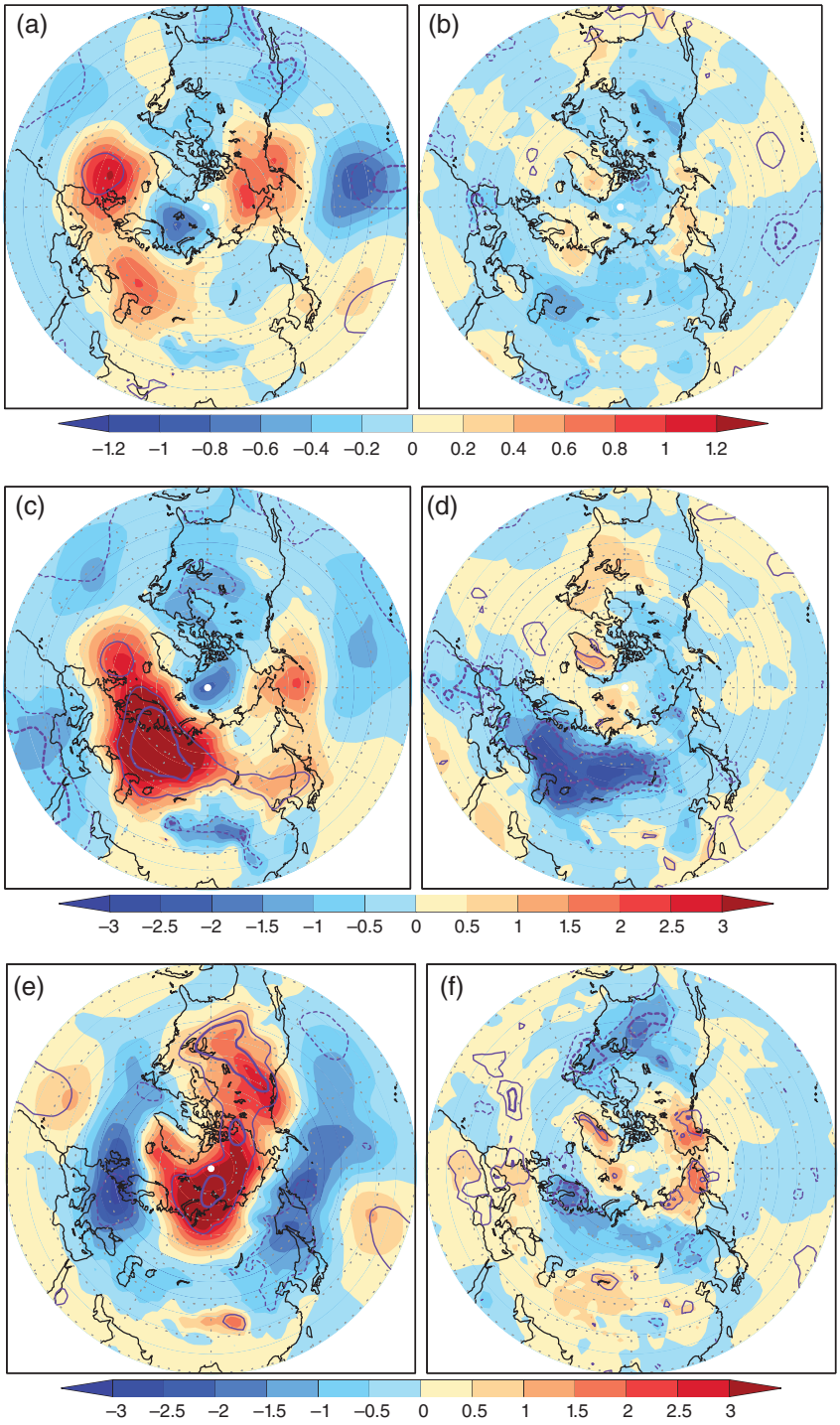

Figure 7. Winter (a) SLP (hPa) and (b) SAT (°C) differences in ensemble means between the LICE/AA and LICE/AC experiments (former – latter). The thin and thick purple contours represent differences at the 0.05 and 0.01 significance levels, respectively. (c), (d) as in (a), (b), but for differences in simulated strong SH winters (SD >1.0). (e) and (f): as in (a) and (b), but for differences in simulated weak SH winters (SD < −1.0). (g) Probability distribution curves of simulated winter mean SATs over the domain in Figure 6(b) (outlined in red) for the LICE/AA (blue) and the LICE/AC (red) experiments. (h) Evolutions of the regionally (outlined in red) averaged winter SATs with ensemble member numbers; the red and blue curves respectively indicate the LICE/AC and LICE/AA experiments.

The simulations capture most patterns in SAT anomalies, except in lower latitudes of Eurasia.

The present study chooses the region (50°–90°E, 40°–50°N) in the mid-latitudes of Eurasia (Figure 6(b), outlined in red) to demonstrate characteristics of winter regionally averaged SAT responses. The reason for selecting this particular region is because it exhibits significant ($p < 0.05$) differences in ensemble means between the two set experiments.

The two sets of experiments display different probability distribution curves (Figure 6(g)). Compared with the HICE/AC experiments, the distribution of simulated

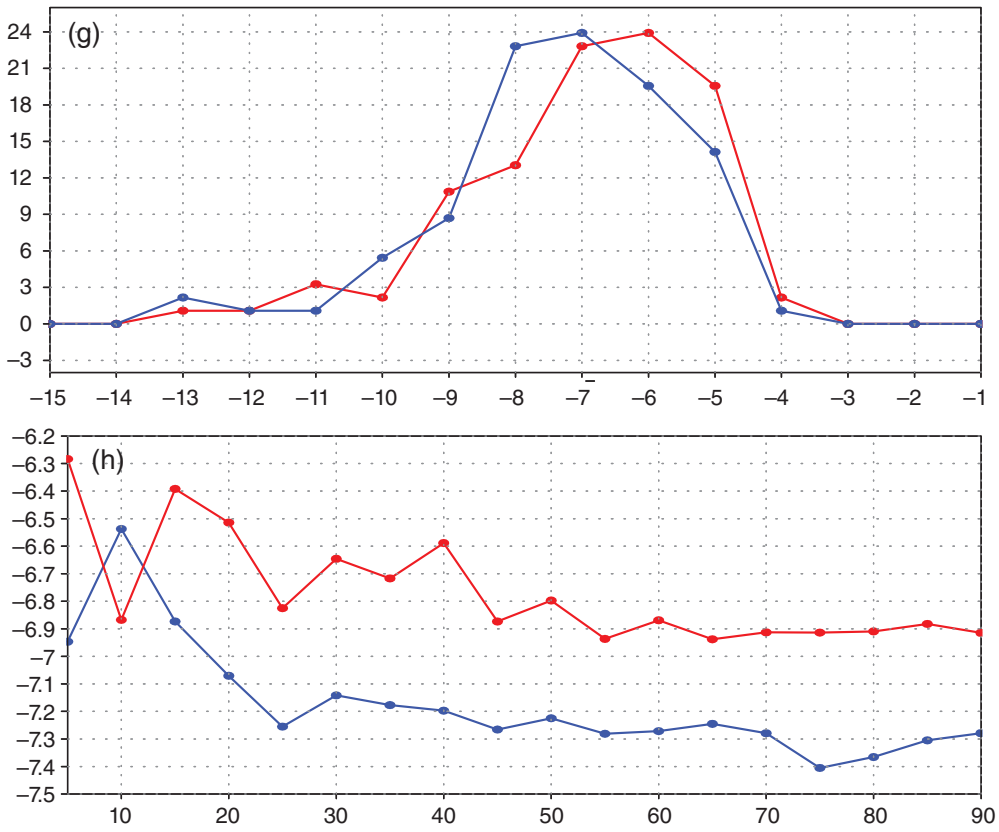

Figure 7. Continued

winter SAT responses for the LICE/AA systematically shifts to lower temperatures. In this region, the difference in ensemble means between two sets of experiments is −0.55 °C (the LICE/AA – HICE/AC) at the 0.05 significance level. Similar probability distribution curves are also observed in a large domain (50°–120°E, 40°–50°N, not shown). Additionally, the number of ensemble members affects winter SAT responses (Figure 6(f)): differences in winter mean SATs between the two sets of experiments are steadily >0.5 °C when ensembles exceed 50 members, and SAT differences are at the 0.05 significance level only when ensembles exceed 75 members. This implies that although atmospheric responses are small in comparison to large atmospheric internal variability (Screen *et al.*, 2013), a robust response is still detectable. Figure 6 clearly indicates that Arctic sea ice forcing produces significant impacts, and significant negative SAT anomalies were observed over Eurasia and the northern North Pacific.

Ensemble means of simulated amplitudes of anomalies are clearly weaker relative to observations, consistent with results of some previous studies (Alexander *et al.*, 2004; Screen *et al.*, 2013, 2014; Mori *et al.*, 2014; Peings and Magnusdottir, 2014). One of the reasons for relatively weak responses may be related to the use of monthly, rather than daily, SIC data as the forcing and also to the lack of interannual regional variability in sea ice loss. In the real world, sea ice losses are larger in one region than another each year, which affects the location and strength of the atmospheric response (see Kug *et al.*, 2015). Moreover, individual ensemble members exhibit stronger responses than the ensemble mean.

Next, the present study examines the impact of atmospheric initial conditions on the winter response to reduced Arctic sea ice. Figure 7 presents differences in ensemble means between the LICE/AA and LICE/AC (former – latter). In both cases, the ensemble-mean SHIs are nearly equal (1030.2 hPa), with SDs of 1.7 (AC) and 1.8 (AA) hPa. Simulated differences in winter mean SLP and SAT are not significant over most of Eurasia (Figure 7(a) and (b)). An AA in summer over the Arctic Ocean contributes dynamically to decreases in autumn sea ice extent because the ice moves to the right of the surface wind, driving the ice poleward. It seems that relative to the AC, the AA enhances the negative feedback of sea ice loss on the winter atmospheric circulation variability over Eurasia, leading to positive SLP and negative SAT anomalies over most parts of Eurasia (Figure 7(a) and (b)). In the North Atlantic and mid-latitudes of the North Pacific, however, SLP anomalies are evident.

If only cases with a simulated SHI > 1.0σ (strong SH) are considered, the AA strengthens the winter SLP further and reduces the winter SAT over Eurasia considerably, relative to the AC (Figure 7(c) and (d)), indicating a stronger winter monsoon. In contrast, in cases with a weak SH (simulated SHIs < -1.0σ), relative to the AC, the AA weakens the winter SLP in the mid- and high-latitudes of Eurasia and strengthens SLP over the Arctic and North America, leading to positive SAT anomalies in the mid-latitudes of the

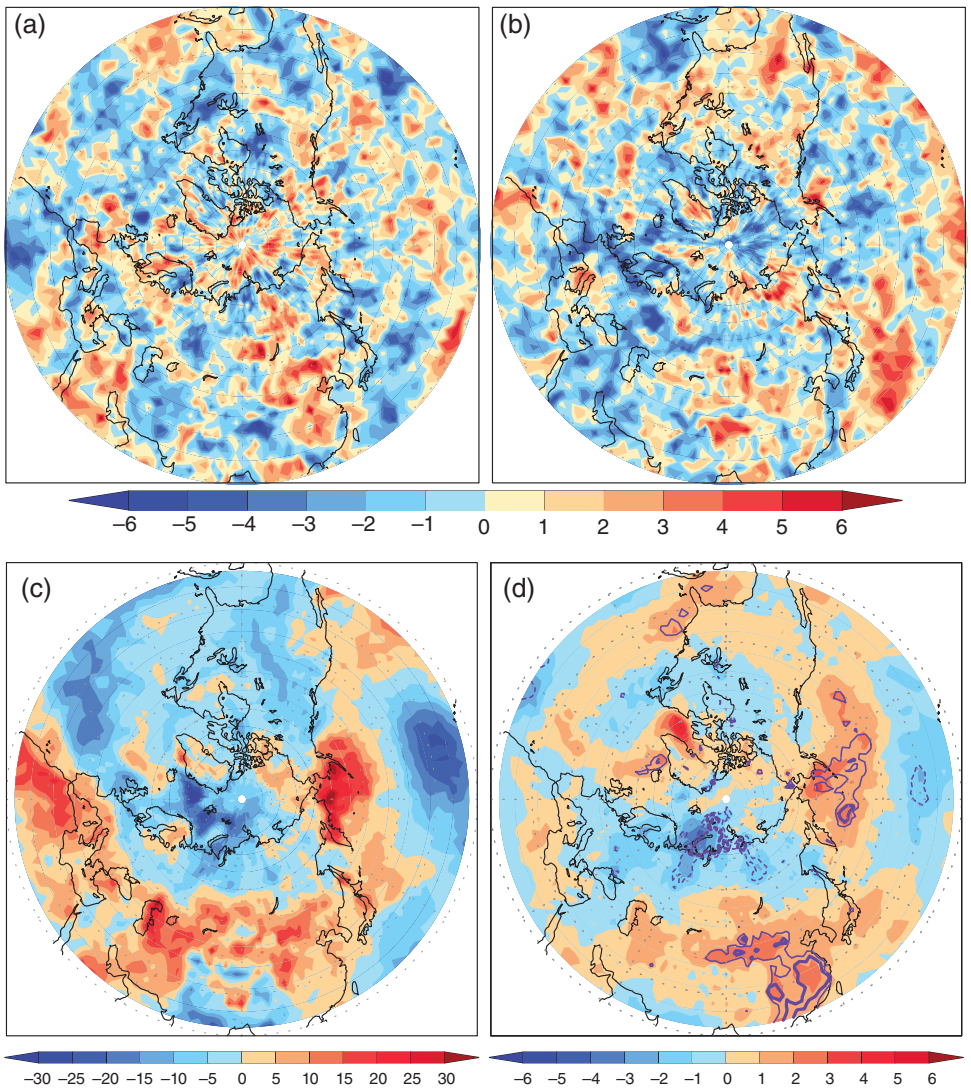

Figure 8. (a) Differences in cumulative winter extreme cold events (SD of simulated winter mean SATs < -1.50) between the LICE/AA and LICE/AC experiments (see text) (former – latter). (b) as in (a), but for winter extreme warm events (SD of simulated winter mean SATs > 1.50). (c) Differences in cumulative winter daily extreme cold events (SD of winter daily SATs < -1.50) between two winters (2011/2012 – 1996/1997). (d) Regression map of cumulative winter daily extreme cold events, regressed on the normalized negative AD wind pattern; data were detrended before performing linear regression analyses. The thin and thick purple contours denote anomalies at the 0.05 and 0.01 significance levels, respectively. Units are frequency.

Asian continent and significant negative SAT anomalies over most of North America (Figure 7(e) and (f)), indications of a weaker winter monsoon.

Probability distribution curves of simulated winter SAT responses demonstrate impacts of different atmospheric initial conditions on atmospheric responses, and the AC initial conditions produce more frequent warm winters relative to the AA initial conditions (Figure 7(g)). Although the difference in ensemble means between the two sets of experiments is −0.30 °C (LICE/AA – LICE/AC) and not significant, their differences are visible (Figure 7(h)).

Figure 7 implies that under the same conditions of reduced sea ice, the AA tends to enhance winter atmospheric circulation variability over Northern Hemisphere continents, thereby increasing the probability of extreme events (Figure 8). Simulation results suggest that, relative to the AC, the AA favours more frequent winter extreme events – both cold and warm over the mid- and low-latitudes of East Asia (Figure 8(a) and (b)) – as reflected in enhanced variability in winter SATs. This does not conflict with the result shown in Figure 7(g). In the selected region (outlined in red, Figure 6(b)), there were eight (5) extreme cold and two (1) extreme warm events for the LICE/AA (LICE/AC) experiments. Moreover, observations reveal an increased frequency of winter daily extreme cold events over the mid-latitudes of the Asian continent and East Asia during the winter of 2011/2012 *versus* the winter of 1996/1997 (Figure 8(c)). Statistical analyses further indicate that the negative phase of the summer AD wind pattern favours frequent occurrences of winter daily extreme cold events over the mid- and low-latitudes of East Asia (Figure 8(d)), consistent with simulation results in Figure 8(a).

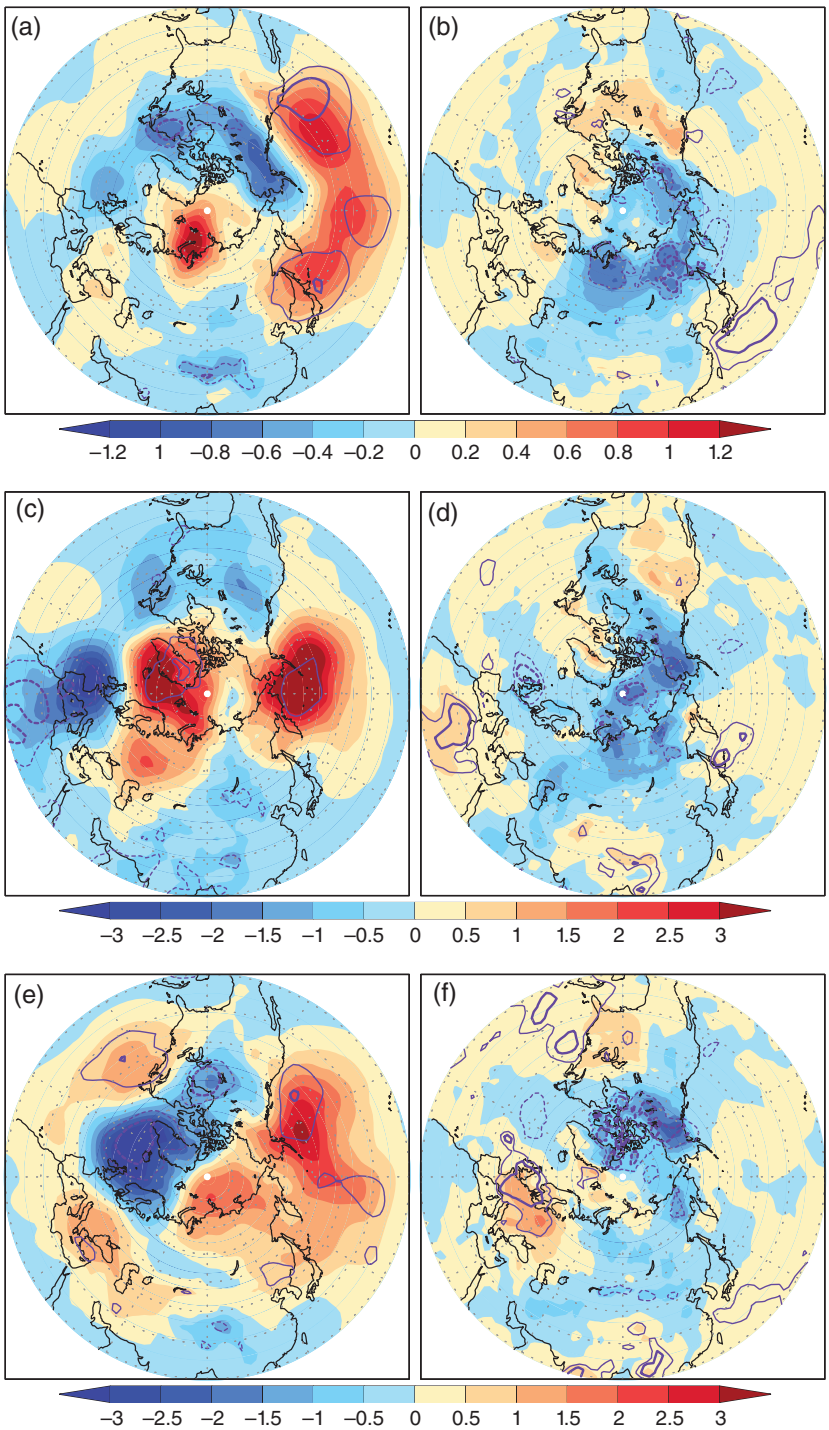

Figure 9. Winter (a) SLP (hPa) and (b) SAT (°C) differences in ensemble means between the HICE/AA and HICE/AC experiments (former − latter). The thin and thick purple contours represent differences at the 0.05 and 0.01 significance levels, respectively. (c), (d) as in (a), (b), but for differences in simulated strong SH winters (SD >1.0). (e), (f) as in (a), (b), but for differences in simulated weak SH winters (SD < −1.0). (g) Probability distribution curves of simulated winter mean SATs over the domain in Figure 6(b) (outlined in red) for the HICE/AA (blue) and HICE/AC (red) experiments. (h) Evolutions of the regionally (outlined in red) averaged winter SATs with ensemble member numbers; the red and blue curves respectively indicate the HICE/AC and HICE/AA experiments.

The same analysis was performed using the HICE forcing with both the AA and AC initial conditions. The ensemble-mean SHIs are also nearly equal: 1030.0 (AA) and 1030.1 (AC) hPa, with SDs of 1.5 (AA) and 1.7 (AC) hPa. Although significant SLP and SAT anomalies are observed over the mid- and high-latitudes of the Northern Hemisphere, it is unclear whether the summer AD wind pattern has a substantial influence on Eurasian winter atmospheric responses under the HICE conditions (Figure 9). Robust responses are, however, exhibited over much of the North Pacific and the Atlantic sector of the Arctic Ocean. Interestingly, the sign of the SLP response

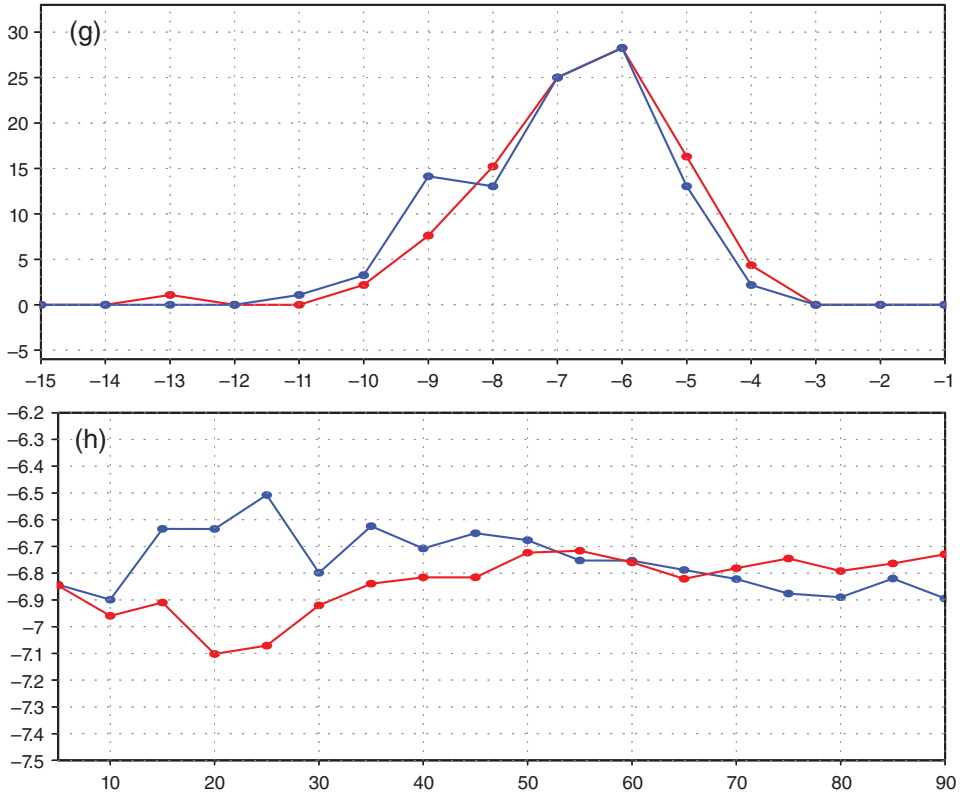

Figure 9. Continued

in the northern North Atlantic is opposite for strong SHI (positive SLP anomaly) versus weak SHI (negative SLP anomaly). It seems that impacts of different atmospheric initial conditions on winter SAT responses become weaker relative to the LICE condition (Figures 7(g) and 9(g)). The difference in ensemble means between the two sets of experiments is −0.18 °C (AA – AC), and differences in their responses are smaller relative to the LICE forcing (Figures 7(h) and 9(h)).

The above analyses suggest that the summer AD wind pattern not only influences Arctic sea ice but also plays an important role in modulating feedback of Arctic sea ice on atmospheric circulation variability during the following winter, particularly in the background of Arctic sea ice loss when the Arctic air–sea–ice interactions become more sufficient; thus, the negative phase of the summer AD wind pattern enhances the negative feedback of sea ice loss on the winter climate and leads to lower SATs in the mid-latitudes of Eurasia, relative to its positive phase.

These simulation experiments also imply that over the Arctic, complex and varying summer circulation patterns obscure linkages between Arctic sea ice loss and large-scale atmospheric responses over Eurasia during the wintertime.

6. Conclusions and discussion

By performing CVEOF analysis of surface wind fields over the Northern Hemisphere, the present study demonstrated that the summer AD wind pattern extends over the entire Arctic as well as the mid-latitudes to 20°N. The negative phase of the summer AD wind pattern is characterized by an anomalous anticyclone over the Arctic Ocean and its marginal seas except for the Barents-Kara seas, where an anomalous cyclone dominates. This wind pattern is significantly associated with the strength of the SH and the frequency of extreme cold events over East Asia during the following winter. The results of the present study suggest that autumn sea ice provides the mechanism linking this summer wind pattern with weather/climate variability over East Asia in the cold season.

Model simulations support observed findings that reduced sea ice favours strengthened winter SLP over most of Eurasia and the northern North Pacific and lower winter SAT in most of Eurasia, leading to a stronger winter monsoon. While simulated amplitudes of anomalies are clearly weaker than in observations, this is expected owing to prescribed monthly SIC data acting as the external forcing and large atmospheric internal variability. Simulations demonstrate that the summer AD wind pattern modulates winter atmospheric responses to sea ice loss. Relative to the positive phase of the summer AD wind pattern, its negative phase enhances the negative feedback of Arctic sea ice loss on the winter atmospheric variability over Eurasia and North America. Thus, the summer AD wind pattern may serve as a potential precursor of the severity of winter weather over Eurasia in the present-day climate background.

As the summer AD wind pattern extends throughout northern mid-latitudes, this wind pattern likely affects

summer SSTs in the Pacific and North Atlantic. If these SST anomalies persist into the following autumn, then they may also contribute to the summer/winter connection. Recent studies suggest that tropical and extra-tropical SST anomalies influence the Arctic and Eurasia climate (Ding *et al.*, 2014; Sato *et al.*, 2014; Simmonds and Govekar, 2014). It has been shown that combined effects of both SST and sea ice anomalies contribute to the winter SH variability (Wu *et al.*, 2011; Lee *et al.*, 2015). Associations between the summer AD wind pattern and Northern Hemispheric SST anomalies in summer and autumn, and the lag-influence of SST anomalies on the winter SH, are topics of further research.

It should be pointed out that the link between the summer AD wind pattern and the strength of the SH is non-stationary, and it depends on chosen study periods. If the period was 1960–2014, their correlation was reduced to be −0.30 at the 0.05 significance level (not shown). During this period, 21-year sliding correlation coefficients between them were not significant prior to the mid-1970s and positive in the beginning of the 1960s (not shown), different from that in Figure 2(d). Thus, this non-stationary relationship may partly reflect an alternation of Arctic cooling and warming periods with low and high Atlantic inflow, an essential feature of the Arctic climate dynamics (Smedsrud *et al.*, 2013). Additionally, this relationship may be also related to the nonlinear response of the atmospheric circulation to sea ice changes (Petoukhov and Semenov, 2010; Semenov and Latif, 2015). Consequently, this non-stationary relationship must be considered before predicting winter SH and East Asian winter monsoon.

Acknowledgements

The authors are grateful to the anonymous reviewers for their constructive and helpful comments, as well as to the British Atmospheric Data Centre (BADC) and the NCEP/NCAR for providing sea ice concentration data and atmospheric re-analysis data. This study was supported by the National Key Basic Research Project of China (2013CBA01804, 2015CB453200), the National Natural Science Foundation of China (41475080, 41221064), the State Oceanic Administration Project (201205007), and NSF/ARCSS grant 1304097(JAF).

References

Alexander MA, Bhatt US, Walsh J, Timlin MS, Miller JD, Scott JD. 2004. The atmospheric response to realistic Arctic sea ice anomalies in an AGCM during winter. *J. Clim.* **17**: 890–905.

Carmack E, Melling H. 2011. Warmth from the deep. *Nat. Geosci.* **4**: 7–8.

Cohen J, Furtado J, Barlow M, Alexeev V, Cherry J. 2012. Arctic warming, increasing snow cover and widespread boreal winter cooling. *Environ. Res. Lett.* **7**: 014007, doi: 10.1088/1748-9326/7/1/014007.

Cohen J, Screen J, Furtado J, Barlow M, Whittleston D, Coumou D, Francis J, Dethloff K, Entakhabi D, Overland J, Jones J. 2014. Recent Arctic amplification and extreme mid-latitude weather. *Nat. Geosci.* **7**: 627–637.

Deser C, Magnusdottir G, Saravanan R, Phillips A. 2004. The effects of North Atlantic SST and sea ice anomalies on the winter circulation in CCM3. Part II: direct and indirect components of the response. *J. Clim.* **17**: 877–889.

Ding Y. 1990. Build-up, air mass transformation and propagation of Siberian high and its relations to cold surge in East Asia. *Meteorol. Atmos. Phys.* **44**: 281–292.

Ding Q, Wallace JM, Battisti DS, Steig EJ, Gallant A, Kim HJ, Geng L. 2014. Tropical forcing of the recent rapid Arctic warming in northeastern Canada and Greenland. *Nature* **509**: 209–212, doi: 10.1038/nature13260.

Francis JA, Vavrus SJ. 2012. Evidence linking Arctic amplification to extreme weather in mid-latitudes. *Geophys. Res. Lett.* **39**: L06801, doi: 10.1029/2012GL051000.

Francis JA, Vavrus SJ. 2015. Evidence for a wavier jet stream in response to rapid Arctic warming. *Environ. Res. Lett.* **10**: 1–12, doi: 10.1088/1748-9326/10/1/014005.

He JH, Wu FM, Qi L. 2015. Decadal/interannual linking between autumn Arctic sea ice and following winter Eurasian air temperature. *Chin. J. Geophys.* **58**: 1089–1102, doi: 10.6038/cjg20150401.

Holloway G, Sou T. 2002. Has Arctic sea ice rapidly thinned? *J. Clim.* **15**: 1691–1701.

Honda M, Inous J, Yamane S. 2009. Influence of low Arctic sea-ice minima on anomalously cold Eurasian winters. *Geophys. Res. Lett.* **36**: L08707, doi: 10.1029/2008GL037079.

Jaiser R, Dethloff K, Handorf D. 2013. Stratospheric response to Arctic sea ice retreat and associated planetary wave propagation changes. *Tellus A* **65**: 19375.

Jhun JG, Lee EJ. 2004. A new East Asian winter monsoon index and associated characteristics of the winter monsoon. *J. Clim.* **17**: 711–726.

Kim BM, Son SW, Min SK, Jeong JH, Kim SJ, Zhang X, Shim T, Yoon JH. 2014. Weakening of the stratospheric polar vortex by arctic sea-ice loss. *Nat. Commun.* **5**: 1–8, doi: 10.1038/ncomms5646.

Kug JS, Jeong JH, Jang YS, Kim BM, Folland CK, Min SK, Son SW. 2015. Two distinct influences of Arctic warming on cold winters over North America and East Asia. *Nat. Geosci.* **8**: 759–762, doi: 10.1038/NGEO02517.

Kwok R. 2009. Outflow of Arctic Ocean sea ice into the Greenland and Barents Seas: 1979–2007. *J. Clim.* **22**: 2438–2457, doi: 10.1175/2008JCLI2819.1.

Laxon S, Peacock N, Smith D. 2003. High interannual variability of sea ice thickness in the Arctic region. *Nature* **425**: 947–950.

Lee S. 2014. A theory for polar amplification from a general circulation perspective. *Asia-Pac. J. Atmos. Sci.* **50**: 31–43, doi: 10.1007/s13143-014-0024-7.

Lee MY, Hong CC, Hsu HH. 2015. Compounding effects of warm SST and reduced sea ice on the extreme circulation over the extratropical North Pacific and North America during the 2013–2014 boreal winter. *Geophys. Res. Lett.* **42**: 1612–1618, doi: 10.1002/2014GL062956.

Liu J, Curry JA, Wang H, Song M, Horton RM. 2012. Impact of declining Arctic sea ice on winter snowfall. *Proc. Natl. Acad. Sci. U. S. A.* **109**: 4074–4079.

Magnusdottir G, Deser C, Saravanan R. 2004. The effects of North Atlantic SST and sea ice anomalies in the winter circulation in CCM3. Part I: main features and storm track characteristics of the response. *J. Clim.* **17**: 857–876.

Mori M, Watanabe M, Shiogama H, Inoue J, Kimoto M. 2014. Robust Arctic sea-ice influence on the frequent Eurasian cold winters in past decades. *Nat. Geosci.* **7**: 869–873, doi: 10.1038/NGEO2277.

Nakamura T, Yamazaki K, Iwamoto K, Honda M, Miyoshi Y, Ogawa Y, Ukita J. 2015. A negative phase shift of the winter AO/NAO due to the recent Arctic sea-ice reduction in late autumn. *J. Geophys. Res.* **120**: 3209–3227, doi: 10.1002/2014JD022848.

Ogi M, Yamazaki K, Wallace J. 2010. Influence of winter and summer surface wind anomalies on summer Arctic sea ice extent. *Geophys. Res. Lett.* **37**: L07701, doi: 10.1029/2009GL042356.

Overland JE, Wang MY. 2010. Large-scale atmospheric circulation changes are associated with the recent loss of Arctic sea ice. *Tellus A* **62**: 1–9.

Overland JE, Francis JA, Hall R, Hanna E, Kim SJ, Vihma T. 2015. The melting Arctic and mid-latitude weather patterns: are they connected? *J. Clim.* **28**: 7917–7932, doi: 10.1175/JCLI-D-14-00822.1.

Park DS, Lee S, Feldstein SB. 2015. Attribution of the recent winter sea ice decline over the Atlantic sector of the Arctic Ocean. *J. Clim.* **28**: 4027–4033, doi: 10.1175/jcli-d-15-0042.1.

Peings Y, Magnusdottir G. 2014. Response of the wintertime Northern Hemisphere atmospheric circulation to current and projected arctic sea ice decline: a numerical study with CAM5. *J. Clim.* **27**: 244–264.

Perlwitz J, Hoerling M, Dole R. 2015. Arctic tropospheric warming: causes and linkages to lower latitudes. *J. Clim.* **28**: 2154–2167, doi: 10.1175/jcli-d-14-00095.1.

Petoukhov V, Semenov VA. 2010. A link between reduced Barents-Kara sea ice and cold winter extremes over northern continents. *J. Geophys. Res.* **115**: D21111, doi: 10.1029/2009JD013568.

Polyakov I, Johnson M. 2000. Arctic decadal and interdecadal variability. *Geophys. Res. Lett.* **27**(24): 4097–4100.

Polyakov I, Timokhov LA, ALexeev VA, Bacon S, Dmitrenko IA, Fortier L, Frolov IE, Gascard JC, Hansen E, Ivanov VV, Laxon S, Mauritzen C, Perovich D, Shimada K, Simmons HL, Sokolov VT, Steele M, Toole J. 2010. Arctic Ocean warming contributes to reduced polar ice cap. *J. Phys. Oceanogr.* **40**: 2743–2756.

Proshutinsky A, Johnson M. 1997. Two circulation regimes of the wind-driven Arctic Ocean. *J. Geophys. Res.* **102**(C6): 12493–12514.

Rigor I, Wallace J, Colony R. 2002. Response of sea ice to the Arctic Oscillation. *J. Clim.* **15**: 2648–2663.

Roeckner E, Bäuml G, Bonaventura L, Brokopf R, Esch M, Giorgetta M, Hagemann M, Kirchner I, Kornblueh L, Manzini E, Rhodin A, Schlese A, Schulzweida U, Tompkins A. 2003. The atmospheric general circulation model ECHAM5. Part I: model description. Report No. 349, Max Planck Institute for Meteorology: Hamburg, Germany, 127 pp.

Sato K, Inoue J, Watanabe M. 2014. Influence of the Gulf Stream on the Barents sea ice retreat and Eurasian coldness during early winter. *Environ. Res. Lett.* **9**: 1–8, doi: 10.1088/1748-9326/9/8/084009.

Screen JA, Simmonds I. 2010. The central role of diminishing sea ice in recent Arctic temperature amplification. *Nature* **464**: 1334–1337, doi: 10.1038/nature09051.

Screen JA, Simmonds I. 2013a. Exploring links between Arctic amplification and mid-latitude weather. *Geophys. Res. Lett.* **40**: 959–964, doi: 10.1002/GRL.50174.

Screen JA, Simmonds I. 2013b. Caution needed when linking weather extremes to amplified planetary waves. *Proc. Natl. Acad. Sci. U. S. A.* **110**: E2327, doi: 10.1073/pnas.1304867110.

Screen JA, Simmonds I, Deser C, Tomas R. 2013. The Atmospheric response to three decades of observed Arctic sea ice loss. *J. Clim.* **26**: 1230–1248.

Screen JA, Deser C, Simmonds I, Tomas R. 2014. Atmospheric impacts of Arctic sea-ice loss, 1979–2009: separating forced change from atmospheric internal variability. *Clim. Dyn.* **43**: 333–344, doi: 10.1007/s00382-013-1830-9.

Semenov AV, Latif M. 2015. Nonlinear winter atmospheric circulation response to Arctic sea ice concentration anomalies for different periods during 1966–2012. *Environ. Res. Lett.* **10**: 054020, doi: 10.1088/1748-9326/10/5/054020.

Serreze M, Holland M, Stroeve J. 2007. Perspectives on the Arctic's shrinking sea-ice cover. *Science* **315**: 1533–1536, doi: 10.1126/science.1139426.

Shimada K, Kamoshida T, Itoh M, Nishino S, Carmack E, McLaughlin F, Zimmermann S, Proshutinsky A. 2006. Pacific Ocean inflow: influence on catastrophic reduction of sea ice cover in the Arctic Ocean. *Geophys. Res. Lett.* **33**: L08605, doi: 10.1029/2005GL025624.

Simmonds I. 2015. Comparing and contrasting the behavior of Arctic and Antarctic sea ice over the 35 year period 1979–2013. *Ann. Glaciol.* **56**(69): 18–29, doi: 10.3189/2015AoG69A909.

Simmonds I, Govekar PD. 2014. What are the physical links between Arctic sea ice loss and Eurasian winter climate? *Environ. Res. Lett.* **9**: 1–3, doi: 10.1088/1748-9326/9/10/101003.

Smedsrud LH, Esau I, Ingvaldsen RB, Eldevik T, Haugan PM, Li C, Lien VS, Olsen A, Omar AM, Otterå OH, Risebrobakken B, Sandø AB, Semenov VA, Sorokina SA. 2013. The role of the Barents Sea in the Arctic climate system. *Rev. Geophys.* **51**: 415–449, doi: 10.1002/rog.20017.

Spreen G, Kwok R, Menemenlis D. 2011. Trend in Arctic sea ice drift and role of wind forcing: 1992–2009. *Geophys. Res. Lett.* **38**: L19501, doi: 10.1029/2011GL048970.

Stroeve JC, Serreze MC, Holland MM, Kay JE, Maslanik J, Barrett AP. 2012. The Arctic's rapidly shrinking sea ice cover: a research synthesis. *Clim. Change* **110**: 1005–1027.

Tang QH, Zhang XJ, Yang XH, Francis JA. 2013. Cold winter extremes in northern continents linked to Arctic sea ice loss. *Environ. Res. Lett.* **8**: 1–6, doi: 10.1088/1748-9326/8/1/014036.

Thompson D, Wallace J. 2001. Regional climate impacts of the Northern Hemisphere annular mode. *Science* **293**(5527): 85–89.

Thorndike AS, Colony R. 1982. Sea ice motion in response to geostrophic winds. *J. Geophys. Res.* **87**(C8): 5845–5852.

Walsh J, Chapman W, Shy T. 1996. Recent decrease of sea level pressure in the central Arctic. *J. Clim.* **9**: 480–486.

Wang J, Zhang J, Watanabe E, Ikeda M, Mizobata K, Walsh J, Bai X, Wu B. 2009. Is the dipole anomaly a major driver to record lows in Arctic summer sea ice extent? *Geophys. Res. Lett.* **36**: L05706, doi: 10.1029/2008GL036706.

Wu B, Wang J. 2002. Winter Arctic Oscillation, Siberian high and East Asian winter monsoon. *Geophys. Res. Lett.* **29**: 1897, doi: 10.1029/2002GL015373.

Wu B, Wang J, Walsh J. 2006. Dipole anomaly in the winter Arctic atmosphere and its association with sea ice motion. *J. Clim.* **19**: 210–225.

Wu B, Su J, Zhang R. 2011. Effects of autumn-winter arctic sea ice on winter Siberian high. *Chin. Sci. Bull.* **56**: 3220–3228, doi: 10.1007/s11434-011-4696-4.

Wu B, Overland J, D'Arrigo R. 2012. Anomalous Arctic surface wind patterns and their impacts on September sea ice minima and trend. *Tellus A* **64**: 18590.

Wu B, Handorf D, Dethloff K, Rinke A, Hu A. 2013. Winter weather patterns over northern Eurasia and Arctic sea ice loss. *Mon. Weather Rev.* **141**: 3786–3800.

Wu B, Walsh J, Liu J, Zhang X. 2014. Dominant patterns of winter Arctic surface wind variability. *Adv. Polar Sci.* **25**(4): 246–260, doi: 10.13679/j.advps.2014.4.00246.

Wu B, Su J, D'Arrigo R. 2015. Patterns of Asian winter climate variability and links to Arctic sea ice. *J. Clim.* **28**: 6841–6858.

Yang LN, Wu B. 2013. Interdecadal variations of the East Asian winter surface air temperature and possible causes. *Chin. Sci. Bull.* **58**(32): 3969–3977, doi: 10.1007/s11434-013-5911-2.

Zhang Y, Hunke E. 2001. Recent Arctic change simulated with a coupled ice-ocean model. *J. Geophys. Res.* **106**: 4369–4390.

Zhang J, Lindsay R, Schweiger A, Steele M. 2013. The impact of an intense summer cyclone on 2012 Arctic sea ice retreat. *Geophys. Res. Lett.* **40**: 720–726, doi: 10.1002/grl.50190.